Evaluation of Iron Nickel Oxide Nanopowder as Corrosion Inhibitor: Effect of Metallic Cations on Carbon Steel in Aqueous NaCl

A. U. Chaudhry[1,†], Vikas Mittal[2], and Brajendra Mishra[1,3]

[1]*Department of Metallurgical & Materials Engineering, Colorado School of Mines, CO. USA*
[2]*Department of Chemical Engineering, The Petroleum Institute, Abu Dhabi, UAE*
[3]*Present address: Metal Processing Institute, Worcester Polytechnic Institute, MA. USA*

The aim of this study was to evaluate the use of iron-nickel oxide ($Fe_2O_3 \cdot NiO$) nanopowder (FeNi) as an anti-corrosion pigment for a different application. The corrosion protection ability and the mechanism involved was determined using aqueous solution of FeNi prepared in a corrosive solution containing 3.5 wt.% NaCl. Anti-corrosion abilities of aqueous solution were determined using electrochemical impedance spectroscopy (EIS) on line pipe steel (API 5L X-80). The protection mechanism involved the adsorption of metallic cations on the steel surface forming a protective film. Analysis of EIS spectra revealed that corrosion inhibition occurred at low concentration, whereas higher concentration of aqueous solution produced induction behavior.

Keywords : *bode, neutral, corrosion, inductive, nyquist*

1. Introduction

In some recent reports, the use of nano-inorganic particles as anticorrosion pigments in polymer coatings have been reported[1-4]. FeNi can be advantageous as anticorrosion pigments as they retain anticorrosion efficiency even exposing aggressive environment[5]. Further, the inhibition action of the inorganic inhibitor on metal substrates can be determined via solution method. In this process, inorganic inhibitors ions are obtained by dissolving in corrosive solution[6]. The inhibition action depends on the solubility of inorganic inhibitor in a corrosive solvent[7].

In coatings usually cations leaching takes place by aggressive electrolyte from incorporated inorganic oxide traveled through coating defects, where they play to suppress the corrosion. The inhibition action of incorporated inorganic pigment mainly starts with the solubility of pigments in a corrosive solution that leads other electrochemical processes acting at coating/metal interface[7]. Sparingly soluble pigments such as chromates have environmental issues and need replacements with particular active inhibitors. The high solubility of inorganic inhibitor in corrosive solution can accelerate the degrading of the coating whereas inhibitor having too low solubility cannot be considered as an active inhibitor. Therefore, there is always a need to find a suitable substitute inorganic inhibitor for polymer coatings that can behave physicochemically and electrochemically. Metallic cations can affect the electrochemical process of corrosion that occurs at the metal surface. Metallic cations have found applications in various processes; hydrogen reaction inhibition by Cd^{2+}, Mn^{2+}, Ce^{4+} [8,9]; titanium and stainless steel corrosion inhibition in passive regions by Fe^{3+} and Cu^{2+} via fostering passivity of these metals by the action of these cations in the cathodic reactions[10-12]; lead anode corrosion inhibition by Co^{2+} ions in sulphuric acid via increasing catalytic activity of surface oxides for oxygen evolution which in turn increases the current efficiency of the oxygen evolution reaction; and hence little current is available for counter anodic reaction[13], corrosion inhibition of iron by reducing corrosion promoting species using Sn^{2+} ions in acid pickling process[14]. The interaction of certain metallic cations with metal surface can suppress either cathodic, anodic or both the processes.

Present research work deals with the changes occurring at steel surface during interaction with metallic cation from iron-nickel oxide nanopowder. We used two concentration of metal cations obtained from iron-nickel oxide nanopowder and conducted EIS studies for API 5L X80 (carbon steel) immersed in 3.5 wt.% NaCl.

† Corresponding author: cusman@mines.edu

Table 1. Properties of aqueous solutions and solutions

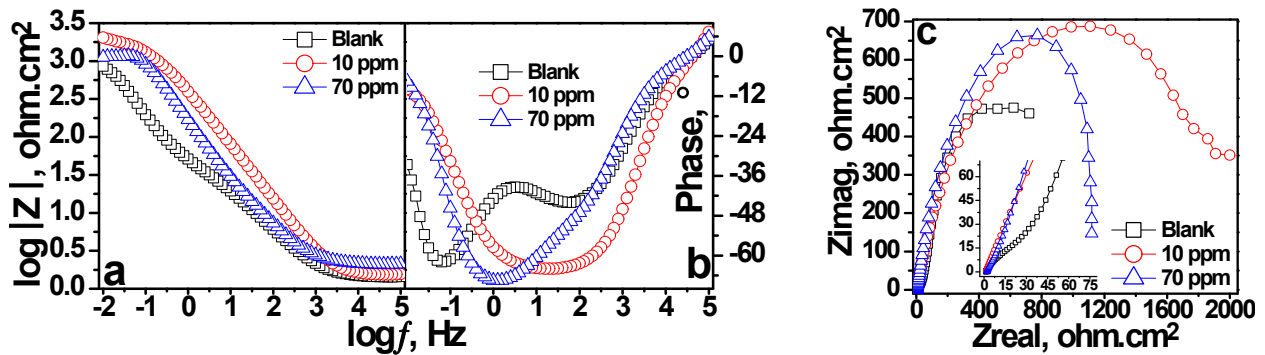| Concentration ppm	pH (±0.05)	Conductivity (mS/cm) (±0.5)	Oxidation Reduction Potential (mV) (±2)	Temperature °C (±0.3)	O$_2$ concentration (ppb) (±10)
Concentrated aq. sol.	8.90	51.0	-114		7080
Blank	6.72	48.2	+14	20	7420
10	7.30	48.6	-16		7208
70	7.70	49.2	-45		7115

Fig. 1. (a-b)Bode and (c) Nyquist plots recorded after 5 hours immersion in 3.5 wt.% NaCl.

2. Experimental

Nano-powders of Fe$_2$O$_3$.NiO (99.9 %, weight) with average particle size 100 nm and density 5.368 g/cm^3 were purchased from American Elements, USA and used as received. A concentrated aqueous solution was prepared by adding 6 g to 1 L to 3.5 wt.% NaCl by shaking on alternative days continuously for 30 days (low solubility of powder in water) followed by decanting to obtain the aqueous solutiion[15]. The stock solutions were further diluted to various concentrations. The properties of aq. sol. solutions were measured as shown in Table 1.

The low conductivity (Table 1) of the aq. sol. showed low solubility of ferrites in water whereas Oxidation reduction potential (ORP) values represent that addition of aqueous solution to the blank solution (dilution) changes the oxidizing nature of solution into reducing. This behavior indicates that although the solubility of the FeNi is low in the water but enough to change the nature of solution which might lead to the inhibition process. For a neutral solution, the combined concentrations of metallic cations (Ni, Fe) in aqueous solution were determined using inductively coupled plasma molar mass spectrometry (ICP-MS) and diluted further accordingly (0, 10 ppm, 70 ppm). A three-electrode cell assembly (Fig. 2) consisting of working electrode as API-5L X80 (Elemental composi-

tion: C 0.07 (weight) %, Mn 1.36 %, Ti 0.008 %, S 0.003 %, P 0.004 % and remaining iron), machined to 10 × 10 × 4 mm, and embedded in epoxy (Fig. 2) was used. A graphite rod as the counter electrode (CE) and for reproducibility, a saturated calomel electrode as reference electrode (RE) was also used. Open circuit potential (OCP) for 5 hours followed by EIS from 10^5 to 10^{-2} Hz at 10 mV AC amplitude were measured using Gamry 600 potentiostat/galvanostat/ZRA at room temperature. Weight losses of the samples were done for 320 hours of immersion and corrosion products were removed with 600 emery papers until shine.

3. Results and discussion

EIS results are presented as Bode plots and Nyquist (Fig. 1 (a-c)) whereas two kinds of equivalent circuits (Fig. 2 (a-b)) were used to extract the electrochemical parameters. For blank solution phase angle exhibits two-time constants at low and intermediate frequency corresponding to charge transfer and outer porous and loose layer. The model circuit elements given in Fig. 2a shows outer layer resistance and capacitance by R$_{out}$ and C$_{out}$ whereas double layer resistance and capacitance are given by R$_{cl}$ and C$_{cl}$. The general value of capacitance was calculated from constant phase element (CPE) parameters using
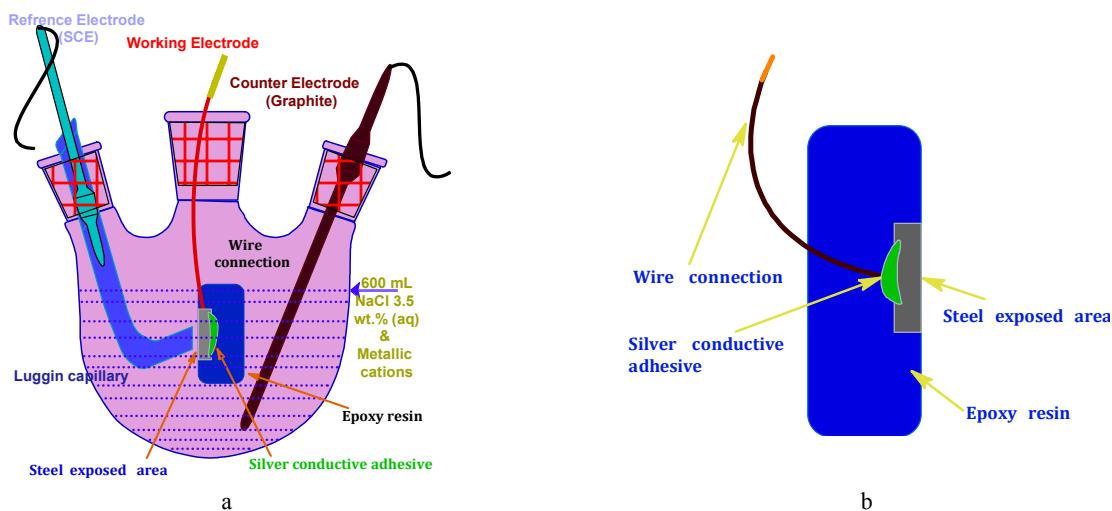
Fig. 2. a) Electrochemical Cell setup and b) epoxy embedded working electrode.
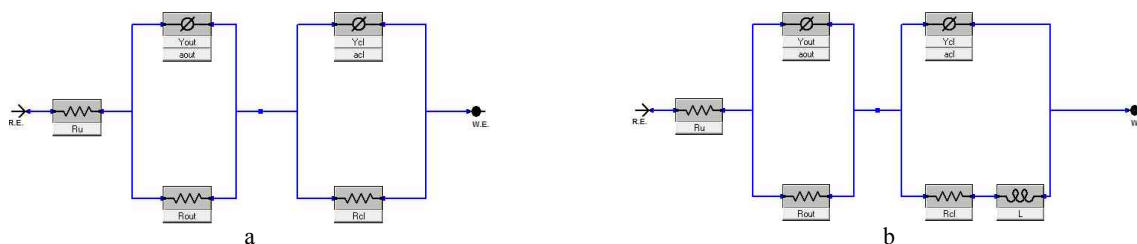

Fig. 3. A representative circuits used to model the EIS (a) Blank & 10 ppm and (b) 70 ppm.

following general mathematical equation:

$$C = Y_o (w'')^{(1-a)}$$

Where C is capacitance, Yo is CPE constant it shows the avaiable surface area for the electrochemical reaction [16], w'' is the frequency found at the maximum of the imaginary part of the impedance, Z'', n is the exponential term which can vary between 1 for pure capacitance and 0 for a pure resistor and also the value of n is measure of surface in inhomogeneity; the higher is its value, the lower is the surface roughening substrate[17]. Usually, in the neutral solution containing sodium chloride, iron develops different kind of surface oxides owing to the anodic dissolution that partially protects it against the severe attack of chloride anions. The higher frequency (HF) region of Nyquist's plot (Fig. 1c) for blank solution shows a slight flattening corresponding to peripheral layer resistance has a value of ~ 66 $\Omega.cm^2$ indicating porous and pervious layer deposits having relatively lower capacitance value (7.19×10^{-4} $F.cm^2$). Intermediate (IF) and low-frequency region (LF) show a mixed i.e. dominant

capacitive and recessive mass transport restricted behavior corresponding to charge transfer resistance (R_{cl}) $\sim$ 1040 $\Omega.cm^2$ and 7.98×10^{-3} $F.cm^2$. The higher value of double layer capacitance (C_{dl}) can be attributed towards the higher degree of surface area available for corrosion as indicated by the higher value of CPE constant (Y_o) owing to the distribution of reaction rate with the location on the electrode surface[18]. Upon addition of small quantity of metallic cations obtained from iron nickel oxide nanopowder i.e. 10 ppm, outer layer resistance increased to 495 $\Omega.cm^2$ and corresponding capacitance also increased dramatically i.e. $\sim 1.9 \times 10^{-3}$ $F.cm^2$. Phase angle for 10 ppm showed conversion of two times constant into a single and broad phase angle peak at medium to low frequency. This behavior suggests the interaction of two-time constants occur owing to compact and stable outer film[19]. This response shows the adsorbed intermediate formed by metallic cations along with surface oxides that lead to the formation of enough stable outer layer with higher resistance. Using Evan's drop experiment, Miszczyk et al. showed that nickel zinc ferrites (NZF) have the ability to create precipitate even at low solubility
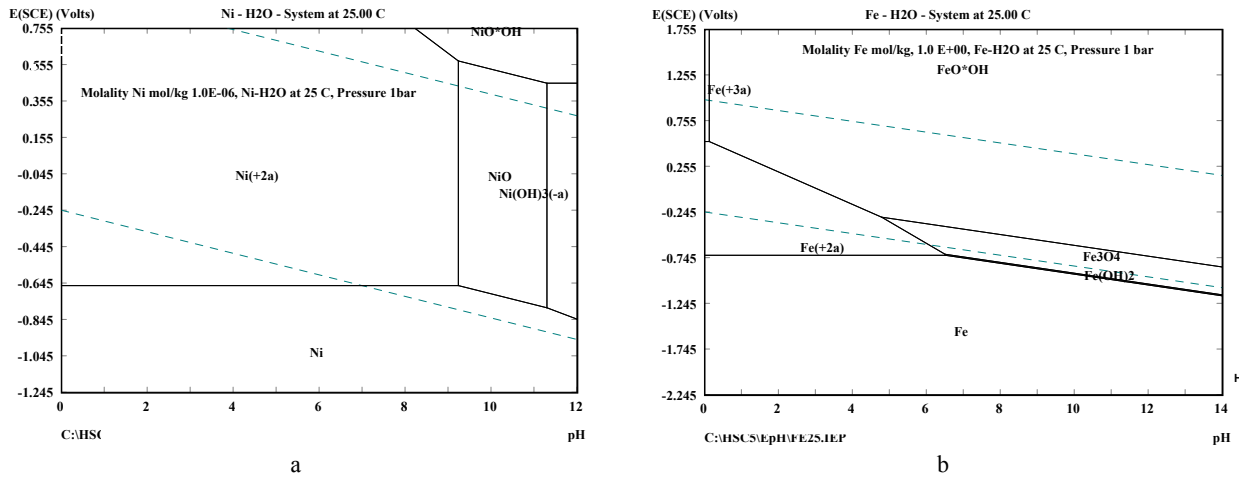
Fig. 4. Pourbaix diagrams showing different stable phases for a) Nickel and b) Iron drawn.

Table 2. OCP and EIS parameters, during 5 hours of immersion in 3.5 wt.% NaCl

Concentration ppm	OCP (mV)	R_{out} (Ω. cm²)	R_{cl} (Ω. cm²)	Y_{out} (sⁿ / Ω. cm²) 10^{-3}	a_{out}	C_{out} (F.cm²) 10^{-4}	Y_{cl} (sⁿ / Ω. cm²) 10^{-3}	a_{out}	C_{cl} (F.cm²) 10^{-3}	L (H.cm²) 10^{3}	Weight Loss (mg)
Blank	-680	65.5	1041	4.10	0.61	7.19	9.46	0.96	7.98	-	14.4, ±0.1
10	-661	495	1679	5.79	0.76	18.9	0.63	0.75	0.20	-	10, ±0.8
70	-651	243	1120	3.98	0.99	38	2.28	0.68	1.02	3.38	19.3, ±0.2

as shown by low conductivity. They showed that drop containing aq. sol. of NZF develop the local anodic site at the center and a cathodic site near the edge of drop and[20,21]. The mechanism of forming these sites was explained by Evan[22]. By the alkaline nature of aq. sol. (Table 1) and in the presence of metallic cations M, the proposed reaction occurring at the steel surface was given by Miszczyk et al. is as follow[21]

$$yM^{2+} + (3-y)Fe^{2+} + 6OH^- \rightarrow M_y Fe_{(3-y)}(OH)_6$$
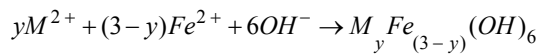
From, Pourbaix diagram[23] of iron (Fig. 4b), the stable phase at pH above 7 can be found as $Fe(OH)_2$ which may co-deposit with the metal cation. Along with the above reaction, Zhao et al. have also explained the corrosion inhibition process at a low concentration of metallic cations. Adsorption of metallic cations having higher electrode potential ($E_{O2/H2O} > E_{Ma+/M} > E_{Fe2+/Fe}$) can lead the following oxidizing-reducing reaction[24]

$$M^{+a} + Fe \rightarrow M + Fe^{+2}$$
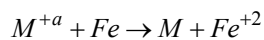
The above reaction can produce electrodeposition of

metallic ion on the iron surface forming a protecting film. Further, from the Pourbaix diagram[23] (Fig. 4a) of nickel, Ni was found as a stable phase above pH of 7. The resultant R_{cl} upon addition of 10 ppm became high i.e. ~ 1680 Ω.cm² showing indeed lower capacitance (0.2×10^{-3} F.cm²) as compare to blank. The addition of a relatively large amount of metallic cations i.e. 70 ppm, phase angle at the low to medium frequency exhibiting narrower peak shifting towards low frequency. This process can be observed better at Nyquist plot where a long inductive loop can be seen at medium to low frequency. Induction loop at intermediate and lower frequency indicate the relaxation of adsorbed intermediates that may result in the corrosive attack of exposed area. In the model circuit (Fig. 3b) it can be seen as L whose impedance can be calculated as:

$$Z(L) = Lwj$$

The inductive behavior due to adsorption can be defined as L = Rτ where τ represents the relaxation time for adsorbed species at the working electrode[17].

Along with the above explanations about inductive behviour, Zhao et al. also explained that at higher concentration of metallic cations, a part of a thicker film formed

due to adsorption of cations may fall into solution, which can result in the development of galvanic cell between exposed surface and adsorbed metallic cations[24]. The capacitance of the outer layer became very high (0.3×10^{-3} F.cm^2) confirming the larger amount of adsorbed species on the surface whereas Rout (243 Ω.cm^2) and Rcl (1120 Ω.cm^2) is decreasing as compared to 10 ppm. These results are by the weight loss measurement after immersion for 320 hours in 3.5 wt.% NaCl containing a different concentration of metallic cations.

4. Conclusions

Corrosion inhibition ability of aq. sol. from iron nickel oxide nanopowder was studied by EIS in 3.5 wt.% NaCl solution. At low concentration, aq. sol. has shown protective ability owing to the formation of a compact and stable film on the steel surface indicated by the single full hump in phase angle. This behavior can be attributed to the adsorbed metallic cations at the steel surface taking part in the surface reactions. The resistance of the protective layer first increases up to 7.5 times and upon addition of a large number of cations it decreases to 3.5 times. At the higher concentration, the inductive phenomenon can be observed as shown by an inductive loop at Nyquist plot owing to the relaxation of adsorbed intermediate. These studies showed that iron nickel oxide has possible application as an anticorrosion pigment in polymeric coatings.

References

1. M. R. Bagherzadeh and F. Mahdavi, *Prog. Org. Coat.*, **60**, 117 (2007).
2. P. P. Mahulikar, R. S. Jadhav, and D. G. Hundiwale, *Iran. Polym. J.*, **20**, 367 (2011).
3. K.-C. Chang, W.-F. Ji, M.-C. Lai, Y.-R. Hsiao, C.-H. Hsu, T.-L. Chuang, Y. Wei, J.-M. Yeh, and W.-R. Liu, *Polym. Chem.*, **5**, 1049 (2014).
4. C. M. Santos, K. Milagros Cui, F. Ahmed, M. C. R. Tria, R. A. M. V. Vergara, A. C. de Leon, R. C. Advincula, and D. F. Rodrigues, *Macromol. Mater. Eng.*, **297**, 807 (2012).
5. A. Kalendová, *Prog. Org. Coat.*, **38**, 199 (2000).
6. A. Amirudin, C. Barreau, R. Hellouin, and D. Thierry, *Prog. Org. Coat.*, **25**, 339 (1995).
7. M. J. Pryor, *J. Electrochem. Soc.*, **101**, 141 (1954).
8. S. Sathiyanarayanan, C. Jeyaprabha, S. Muralidharan, and G. Venkatachari, *Appl. Surf. Sci.*, **252**, 8107 (2006).
9. D. M. Dražić and L. Ž. Vorkapić, *Corros. Sci.*, **18**, 907 (1978).
10. R. A. Covert and H. H. Uhlig, *J. Electrochem. Soc.*, **104**, 537 (1957).
11. A. D. McQuillan and M. K. McQuillan, Titanium, Butterworths Scientific Publications, London (1956).
12. D. Schlain and J. S. Smatko, *J. Electrochem. Soc.*, **99**, 417 (1952).
13. M. Rey, P. Coheur, and H. Herbiet, *Trans. Electrochem. Soc.*, **73**, 315 (1938).
14. H. Leidheiser, *Corrosion*, **36**, 339 (1980).
15. I. M. Zin, *J. Mater. Sci.*, **36**, 450 (2000).
16. J. L. Mora-Mendoza and S. Turgoose, *Corros. Sci.*, **44**, 1223 (2002).
17. A. U. Chaudhry, V. Mittal, and B. Mishra, *Mater. Chem. Phys.*, **163**, 130 (2015).
18. A. Bonnel, F. Dabosi, C. Deslouis, M. Duprat, M. Keddam, and B. Tribollet, *J. Electrochem. Soc.*, **130**, 753 (1983).
19. S. L. d. Assis, S. Wolynec, and I. Costa, *Electrochim. Acta*, **51**, 1815 (2006).
20. C. Chen and F. Mansfeld, *Corros. Sci.*, **39**, 409 (1997).
21. A. Miszczyk and K. Darowicki, *Anti-Corros. Method. M.*, **58**, 13 (2011).
22. U. R. Evans, The corrosion and oxidation of metals: scientific principles and practical application, Edward Arnold, London (1960).
23. M. Pourbaix, Atlas of electrochemical equilibria in aqueous solutions, 2nd English ed., Natl. Assoc. of Corrosion Engineers, Houston, TX (1974).
24. G. N. Mu, T. P. Zhao, M. Liu, and T. Gu, *Corrosion*, **52**, 853(1996).